Unveiling the First Neobatrachian (Anura) Discovered in the paleokarst system of Bolt's Farm (Plio-Pleistocene; Cradle of Humankind), South Africa

Alfred Lemierre, Nonhlanhla Vilakazi, Dominique Gommery, Lazarus Kgasi

AFRICAN JOURNAL OF HERPETOLOGY
https://doi.org/10.1080/21564574.2024.2351821

Unveiling the First Neobatrachian (Anura) Discovered in the paleokarst system of Bolt's Farm (Plio-Pleistocene; Cradle of Humankind), South Africa

Alfred Lemierre [a], Nonhlanhla Vilakazi [b,c], Dominique Gommery [a,c,d] and Lazarus Kgasi [c,d]

[a]Centre de Recherche en Paléontologie - Paris (CR2P, UMR 7207), MNHN/CNRS/SU, Muséum national d'Histoire naturelle, Paris, France;
[b]Department of Zoology, University of Johannesburg, Johannesburg, South Africa;
cHRU and Plio-Pleistocene Palaeontology Section, Ditsong: National Museum of Natural History, Pretoria, South Africa;
[d]Palaeo-Research Institute, University of Johannesburg, Johannesburg, South Africa.

Abstract
Anurans are widely diversified in South Africa, with more than 150 recognised species across the country. However, most the known fossil records of anurans are concentrated in the southern part of South Africa, within the rich Pliocene site of Langebaanweg. Isolated anuran elements have been recovered in the Pliocene deposits of the Cradle of Humankind, but none from the multi-localities site of Bolt's Farm (Plio-Pleistocene). A small block containing an articulated anuran specimen was recently discovered from the Milo A site from Bolt's Farm. We analysed this specimen using CT-scanning to describe its osteology. Surprisingly, the cavity housing the skeleton took the shape of the body of the individual, revealing a small sized individual with a triangular-shaped head. The preserved skeletal elements (around 50% of the skeleton) shows clear synapomorphies of the Ranoidea. A comparison between our specimen and members of all South African ranoid families allow us to highlight numerous osteological similarities between our specimen and taxa of the Pyxicephalidae, leading to a putative attribution to this large African family. In addition, the position of the body is identical to the position of a dormant pyxicephalid, suggesting that our specimen died during a dormancy period, in the dry season. This supports the current paleoenvironment reconstruction, an open savannah with marked seasonality.

Keywords
Anura; Tomography; South Africa; Pleistocene; Cradle of Mankind; Osteology; Neobatrachia

Introduction

South Africa is currently home to more than 150 species of anurans spread throughout the country, and inhabiting various habitats including rivers, mountains, desert, and savannah (Channing and Rödel 2019). Most South African anurans belong within the Neobatrachia – a clade composed of almost all extant anurans worldwide (96% of extant anuran diversity; Frost et al. 2006), with three taxa assigned to the Pipidae (a family of exclusively aquatic anurans), all of which belonging to the genus *Xenopus* Wagler, 1827. In the fossil record, anurans appear in South Africa during the end of the Mesozoic, represented by two pipimorphs (stem-group of Pipidae; Gómez 2016), *Vulcanobatrachus mandelai* Trueb et al., 2005 (Campanian; Gardner and Rage 2016) and *Eoxenopoides reuningi* Haughton 1931 (Maastrichtian; Gardner and Rage 2016). Neobatrachians are absent from the fossil record of South Africa until the Pliocene (Van Dijk 2003; Matthews et al. 2016; Gardner and Rage 2016; Matthews et al. 2019; Matthews and Steininger 2023). This reduced fossil record shows that South African neobatrachians are phylogenetically diverse and distinct from other anuran communities (Matthews et al. 2015; Gardner and Rage 2016; Matthews and Steininger 2023). Unfortunately, the number of studies on neobatrachians from South Africa remains poor, mostly centred on the fossil-rich site of Langebaanweg (south-western Cape region; Matthews et al. 2015, 2016, but see Matthews and Steininger 2023 for description of anurans from the Cradle of Humankind (CoH), and several endemic genera (and families) lack a fossil record.

As South Africa went through several marked climatic and environmental changes since the Mio-Pliocene (with the establishment of a Winter Rainfall Zone along southwestern and the southern tip of South Africa; Matthews et al. 2015, 2016), studying the evolution of anuran communities could help understand the current climate change that extant anurans are currently facing. As an example, study of the Pliocene anuran diversity of Langebaanweg allowed for more precise paleoenvironmental reconstruction, with the presence of summer rainfall in the region (Matthews et al. 2016).

Within South Africa, the CoH represents an exceptional window into the evolution of a Plio-Pleistocene faunal assemblage. It represents a vast assemblage of sites spread throughout northern South Africa (Brain 1981; Hanon et al. 2019; Figure 1A) and was recognised as an UNESCO World Heritage Site in 1999. The CoH represents an assemblage of 12 palaeontological and archaeological sites, the most famous being the Sterkfontein cave which yielded an important collection of australopithecines and other hominins (Broom 1936; Reynolds and Kibii 2011). Among them, the palaeokarst system of Bolt's Farm represents the southernmost locality and houses the oldest sites (Thackeray et al. 2008; Edwards et al. 2019). Bolt's Farm is composed of more than 30 sites, spread on two properties (Gommery et al. 2012; Edwards et al. 2019). Most sites within Bolt's Farm are remnants of mining activities during the late 19th and early 20th centuries (Edwards et al. 2019). The Bolt's Farm sites are composed of pits and represent a Plio-Pleistocene karstic assemblage (Cooke 1991). Within these pits, a diverse mammal fauna has been identified over decade (Sénégas et al. 2002; Thackeray et al. 2008; Gommery et al. 2012; Pickford and Gommery 2020). The study of the preserved fauna offers a unique window into their evolution in the last millions of years, when the region progressively became more arid and desertic (Thackeray et al. 2008). Among the different sites, Milo A was discovered on the 4th of May 2010 (with the identification of mammal fossils; see Gommery et al. 2012), and represents a witness of a larger paleokarst infill where the roof has been eroded (Figures 1B, C). The modern karst system is still forming underground in Palaeoproterozoic dolomites of the Malmani Subgroup (Chuniespoort Group, Transvaal Supergroup). The palaeokarst infill is made up of indurated sediments including fossils (fossiliferous breccia) and speleothems. Like many sites in the CoH, Milo A was mined for

speleothems by the gold industry in the 19th century and the beginning of the 20th century (Brain 1958, 1981). Theseactivities affected only the north-west area and weakly. Since its discovery, regular digs are conducted by the Human Origins and Past Environments Research Unit (HRU) team of the Ditsong: National Museum of Natural History to collect more fossil specimens and achieve a better understanding of the taphonomy of Milo A. While a terminal Pliocene age was originally proposed, using suid biochronology, a recent study has instead proposed an Early Pleistocene age, around 1.8 Ma (Pickford and Gommery 2020). Additionally, the presence of *Eurygathohippus* and *Equus capensis* (taxa of Equidae) also suggests this Early Pleistocene age (pers. com. J. Brink†). During fieldwork in 2011 (for more information, see Materials and methods), a large block of breccia was unearthed. As several mammal remains, including a bovid premolar, were visible, the block was collected to study of these specimens. However, as preparation and cleaning of the block began in 2011, a cavity housing small translucent bones became visible. These bones were assigned to an anuran. This discovery was unexpected, as only isolated anuran bones have been identified in the entire fossil record of the CoH (and remain understudied; pers. com. T. Matthews in Matthews et al. 2019). Thus, it was decided to describe and identify the anuran of Milo A to expand the faunistic list of Milo A and Bolt's Farm (apart from an *Agama* specimen, only mammals have been described; Vilakazi et. al. 2020). As the anuran skeleton was fragile, it was decided to CT-scan the specimen to prevent any damage.

Materials and Methods

Specimen from Milo A (MA) 11-3 is a partially articulated anuran skeleton preserved in a 10.66 cm × 6.92 cm breccia block. The block was much larger when discovered and received the number MA 11-3. It was unearthed on the 19/04/2011 in the South East section of Milo A. The discovery was made by D. Gommery, L. Kgasi and S. Potze during fieldwork undertaken by the HRU team aimed at removing grass and isolated breccia blocks on the surface for future paleontological excavations. As mentioned above, the block was collected due to mammal remains present on it. When the cavity and the anuran bones were identified, the block was separated in two sections, one with the mammal remains (which was then prepared using acetic acid) and a second with the cavity which has retained the number MA 11- 3. The specimen is stored within the Plio-Pleistocene Palaeontology section of the collection of the Ditsong: National Museum of Natural History (Pretoria, South Africa). In addition, we used several comparative specimens of South African anurans (Table S1). We used 3D models of the skeleton of 33 South African taxa (species) for osteological comparisons to the articulated skeleton preserved in MA 11-3.

CT-scan and 3D model

MA 11-3 was micro-CT scanned at the South African Nuclear Energy Corporation (NECSA; Brits, South Africa) using a Nikon XTH 225 ST micro-focus X-ray tomography scanner. A microfocus beam of 130 kV of the CT scanner was used with the following parameters: voltage, 130 kV; current, 100 μA; voxel size, 0.04125 μm; slice resolution, 1466 × 1832 pixels. A total of 1541 virtual slices showing internal structures were reconstructed using XAct (RX solution). Each stack of slices produced was imported in the 3D reconstruction software Mimics 21.0 (Materialise, Leuven, Belgium); before importation, slices were cropped to remove empty spaces. The resulting slices have an image resolution of 404 × 741 pixels and a voxel size of 0.04125 μm for the volume size. 3D models were produced by segmenting each element using the 'thresholding' function (using the contrast on greyscale images). A 3D model of the endocast was produced by segmenting each element using the "add" function. We used the same voxel resolution of 0.04125 μm, with a smoothing factor of 3 for one iteration, to homogenise the model resulting from the segmentation. Data produced by segmentation were

exported in the software 3matic 9.0 as separate files and uploaded on MorphoSource (Table S2). Measurements were taken on the 3D models using the "measure" tool within the software 3matic 9.0.
The nomenclature used for the anatomical description is that of Roček (1980) and Sanchíz (1998). When the process was not named in any of the two, we used the anglicised version.

Systematic Palaeontology
ANURA Duméril, 1805
NEOBATRACHIA Reig, 1958
Ranoidea Rafinesque, 1814
?Pyxicephalidae Tschudi, 1838

Description
MA 11-3 represents an incomplete articulate anuran skeleton, exposed in ventral view (Figure 2A). Most of the preserved bones are glossy, translucent, and partially eroded (Figure 2A). The specimen preserves part of the skull and forelimbs, fragments of pectoral and pelvic girdles, most of the vertebral column and hindlimbs (Figures 2A, 3). In addition, the body shape of the individual was partially preserved within the cavity, as well as several endocranial cavities within the head (Figure 2B).

Body shape
The preserved body shape and bones allow measurements of its snout to vent length, estimated around 33.2 mm. The head is triangular, narrowing anteriorly (16.4 mm wide near the otic region to 6.4 mm on the snout). The head is larger (16.4 mm) than long (13.6 mm). Interestingly, the head of MA 11-3 is high, thinning near the snout (Figure 2B). Thus, the head is slightly wedge-shape in lateral view (Table S2).

Soft tissues
Imprints of several cranial cavities are preserved within the specimen (Figure 2B). The nasal capsules expand anterolaterally when exiting the sphenethmoid region (Figure 2B). Posteriorly, the two capsules and olfactory nerves pathways are not preserved as distinct elements (Figure 2B). No structures are preserved within the main endocranial cavity (Figure 2B). Mid-length of the main endocranial cavity, a pair of slightly ovoid structures expand laterally (Figure 2B). These structures are the imprint of the orbit cavities (Figure 2B).

Cranium
The cranium is poorly preserved. Most of the dorsal dermal bones have been eroded (Figures 3, 4A), leaving the endocranial cavity visible. The frontoparietals, nasals, palatines, vomers, premaxillae are not preserved.

Maxilla: The left maxilla is partially preserved (Figure 4B). It is elongated anteroposteriorly (Figure 4B). In lingual view, the lamina horizontalis seems to project lingually on the anterior half length of the maxilla. The crista dentalis is poorly preserved (Figure 4C) but bears teeth (not segmented). A processus frontalis is present on the anterior portion of the maxilla, but its dorsal extension is difficult to assess due to poor preservation (Figure 4B). The maxilla decreases in height posterior to the processus frontalis. No processus zygomaticomaxillaris is present. This indicates that squamosal and maxilla were not articulated. The processus posterior bears a shallow and well-delimited groove lingually (Figure 4C). This suggests the quadratojugal was ossified (Figure 4C). The poor preservation prevents from assessing if an ornamentation was present on the pars facialis of the maxilla.

Squamosal: Both left and right squamosals are incompletely preserved (Figure 4A). On the left squamosal, only the processus posterolateralis is preserved (Figure 4D). It is slender, and its distal end allows for an estimation of the quadratojugal length, at least half of the maxilla (Figure 4D). On the right squamosal, part of the zygomatic ramus is preserved. The ramus is slender and curved ventrally, delimiting part of the orbit (Table S2). Its distal end is free (i.e., not articulated to the maxilla or nasal). No ramus paroticus or processus posterior are preserved, but their absence or presence cannot be assessed due to the poor preservation of the braincase.
Angulosplenial + dentary: Only the right angulosplenial is preserved. The processus coronoidus is dorsoventrally extended and does not extend as a flattened plate (Figure 4E).

The crista paracoronoidea is well-delimited (Figure 4E), while the crista mandibulare externa is not marked (Figure 4E). The sulcus pro cartilagine Meckeli extends on the lateral surface of the angulosplenial and widens posteriorly into a poorly preserved extremitas spatulate (Figure 4E). On the anterior region of the angulosplenial, a small anteroposteriorly elongated element is present (Figure 4E). It covers the lateral surface of the angular. It is interpreted as the right dentary. The mentomeckelian bone is not preserved.

Sphenethmoid: The sphenethmoid is the best-preserved element of the cranium (Figures 4G, H). It is elongated anteroposteriorly with the preserved septum nasi projecting anteriorly (Figure 4H). The septum extends anteriorly and delimits the two nasal capsules preserved on the endocast (Figure 2B). Within the left nasal cavity, the solum nasi protrudes dorsally as a thick bulge (Figure 4G). The left region of the plane anteorbitale is preserved (Figure 4G), and suggests the region was ossified on at least a third of its total length (Figure 4G). Posteriorly of the plane anteorbitale, a paired depression is visible (Figure 4G). This suggests that both palatines were ossified and in contact with the sphenethmoid.

Parasphenoid: The posterior region of the parasphenoid is preserved (Figure 4F). Although its cultriform process is missing, the absence of any suture on the ventral surface of the sphenethmoid (Figure 4G) suggests it (the cultriform process) did not extend anteriorly on the sphenethmoid. The posterolateral processes (subotic alae) are ossified and extend laterally, covering the ventral floor of the otic capsule. On their lateral margin, a notch is preserved (Figure 4F). This suggests that the ramus interior of the pterygoid partially overlaps the parasphenoid.

Exoccipital and prootic: Both exoccipitals and prootics are preserved as a single compound bone. The latter is poorly preserved, with most of its dorsal region difficult to distinguish from the matrix (Figure 4F). The ventral surface of the compound bone is covered by the parasphenoid, while the paired occipital condyles are hidden by the atlas (Figure 4F).

Vertebral column

The vertebral column is arched ventrally, with the centra protruding (Figures 2A, 3). This conditions is likely the result of post-mortem constrictions. The axial skeleton of MA 11-3 is preserved in various condition. The anterior presacral region only preserves the transverse processes of the vertebrae, while the posterior region preserves both centra and transverse processes. The pelvic region preserves both centrum and transverse processes, and the caudal region preserves most of the urostyle (Figure 3). In total, MA 11-3 possesses eight presacral vertebrae, one sacral and a urostyle. The preserved presacral centra are all procelous, except for the centrum of the eight presacral, which is amphicoelous. The sacral vertebra is biconvex (anterior and posterior cotyles). These conditions of the presacral and sacral vertebrae are characteristics of a diplasiocoelous vertebral column (sensu Boulenger 1886).

Atlas: The atlas (first presacral vertebra) is connected to the braincase and both elements cannot be fully differentiated on the model (Figures 2A, 4A). The atlas is short and wider than long. The atlas is procelous, with a small posterior condyle and two anterior occipital cotyles. The occipital cotyles are separated from each other, but seem closely spaced (Type II of Lynch 1971; Figure 2A).

Post-atlantal presacral vertebrae: Vertebrae II–V are only preserved via their transverse processes (Figure 5A). The transverse process of the second vertebra is oriented anteriorly, is slender and does not widen distally (Figure 5A). The transverse processes of the third vertebra are also anteriorly oriented but seem to slightly widen distally (Figure 5A). The fourth presacral vertebra is also known only by its transverse processes (Figure 5A). They are posterolaterally oriented (Figure 5A). The right transverse process does not widen distally (Figure 5A). The fifth presacral vertebra is also preserved by its transverse processes (Figure 5A). They are oriented perpendicular to the vertebral axis (Figure 5A). They do not seem to widen distally. The sixth vertebra is the anterior-most with a preserved centrum (Figures 5A, B). The centrum is elongated anteroposteriorly (i.e., longer than wide) and hourglass-shaped (Figure 5A). The centrum shows an anterior cotyle and a posterior condyle (Figure 5A). The transverse processes are oriented almost perpendicular to the vertebral axis (Figure 5A). They do not widen distally. The seventh vertebra also preserves its centrum. The latter is similar to the centrum of the sixth vertebra (Figure 5A). Only the base of the transverse processes is preserved and is oriented perpendicular to the vertebral axis (Figure 5A). The eighth vertebra preserves both its centrum and base of transverse processes (Figure 5A). The centrum is shorter than those of the sixth and seventh vertebrae (Figure 5A). The centrum bears an anterior and posterior cotyle (Figure 5A). The transverse processes are broken at their base (Figure 5A). Several vertebrae seem to have part of their dorsal region preserved. However, no neural spine is visible. This could suggest that MA 11-3 had a poorly developed neural spine.

Sacral vertebra: This vertebra is strongly sutured with the eight presacral vertebrae. Although their centra are distinct (Figure 2A), it was not possible to segment them as separated models (Figure 5B). The vertebra is short, wider than long (Figures 5A, B). The sacral vertebra bears an anterior condyle (Figure 2A) and two posterior condyles. Thus, the sacro-urostylar articulation is bicondylar. The left sacral transverse process is preserved. It is oriented posterolaterally (Figures 5A, B). The process is cylindrical-like, and slightly widens distally (Figure 5A).

Urostyle: The urostyle bears two anterior cotyles, well separated from each other (Figure 2A). The urostyle also bears a high and well-developed dorsal crest, that extends on the whole length of the bone (Figure 5C).

Pectoral girdle

Most of the pectoral girdle has not been preserved and was likely eroded. Only the scapulae are partially preserved (Figure 3).

Scapulae: Both scapulae are preserved, but the left scapula is poorly preserved, while the right one is almost complete (Figures 5D, E). The scapula is elongated transversally, with a moderately widened distal end of the margin suprascapularis (Figure 5D). Th anterior margin is slightly concave, without a crest (Figure 5D). The posterior margin is also lacking any crest (Figure 5D). The processus acromialis is incomplete but is separated from the small processus glenoidalis by a sinus interglenoidalis (Figure 5D). Although not complete, it is clear the processus acromialis is wider than the processus glenoidalis. In lateral view, the latter processus

is hidden by the former (Figure 5D). In medial view, a medial crest is visible on the processus glenoidalis, and extends up to mid-length of the scapula shaft (Figure 5E). The glenoid fossa is partially preserved but seems moderately extended dorsoventrally (Figure 5E).

Forelimb

Humeri: Both humeri are partially preserved (Figure 3). The humeri bear a ventral crest (Figure 5F). the ventral crest is high and extends from the proximal head to half of the diaphysis (Figures 5F, G). Distally, the eminentia capitata size and shape is difficult to assess, owing to the articulated radioulna (Figure 3). Nevertheless, it seems well ossified and wide (Figure 5F). The eminentia capitata is not shifted from the diaphysis axis. Although badly preserved, the epicondylus ulnaris is clearly more developed than the epicondylus radialus, slightly protruding laterally (Figure 5F). The epicondylus radialus seems barely distinct from the eminentia capitata (Figures 5F, H). A shallow depression above the eminentia could be interpreted as the fossa cubitalis (Figure 5F). On the dorsal surface, a small triangular groove is visible on the distal region of the left humerus (Figure 5H). It is interpreted as the olecranon scar.

Radioulnae: Both radioulnae are preserved. Unfortunately, the contrast between these bones and the matrix is too faint to allow for their segmentation.

Pelvic girdle

Ilia: Only the distal region of each ilia is preserved (Figure 3). No trace of a dorsal crest is preserved.

Hindlimbs

The hindlimbs represent one of the best-preserved regions of MA 11-3. Most of the right hindlimb is preserved within the matrix.

Femora: Only the proximal heads of both femora are preserved (Figures 3, 6A).

Tibiofibulae: Both tibiofibulae are incompletely preserved, but the right one is preserved on its whole length (Figure 3). It is 32 mm long. Tibiofibulae of MA 11-3 are slender and elongated.
Tarsals: Only the tarsals from the right hindlimb are preserved. The tibiale and fibulare are not fused (Figure 6A). The tibitale is complete and 7 mm long. Its diaphysis is sigmoid (Figure 6A). Only the proximal region of the fibulare is preserved (Figure 6A)

Metatarsals: Four metatarsals (digits II, III, IV and V) are preserved (Figure 6B). They are poorly preserved, making their segmentation difficult. It was not possible to separate the metatarsals of digits II, III and IV (Figure 6B). The metatarsal of digit IV is the longest (8.75 mm). The metatarsal of digit II is incomplete, as it was eroded (it is visible on the block; Figure 2A).

Phalanx: The first phalanx of digits III, IV and V are preserved (Figure 6B). They are elongated anteroposteriorly, with the one of digit IV being the longest. Only digit IV has more preserved phalanges. In total, this digit possesses four phalanges (Figure 6B). Its second and third phalanges are slender and smaller than the first phalanx. The terminal phalanx is cone-like, narrowing distally into a tapered end (Figure 6B; state 4 of Clarke 1981). The total length of phalanges of digit IV is superior to the length of its metatarsal (Figure 6B).

Discussion

Taxonomic attribution

A diplasiocoelous vertebral column is considered one of the main synapomorphies of Ranoidea (Duellman and Trueb 1994; Frost et al. 2006). MA 11-3 can thus be referred to the Ranoidea. In South Africa, ten ranoid families are currently recognised (Channing and Rodel 2019; Matthews et al. 2019). We decided to compare MA 11-3 to members (24 genera) of all ten families to test the affinities of our specimens. We also expand the comparisons to include all pyxicephalid genera (a well-diversified family in South Africa; Hime et al. 2021). We also excluded from our comparisons the recently described genus from the Pliocene of Cooper's Cave (Matthews and Steininger 2023), as the available osteological information cannot be compared to our specimen.

MA 11-3 is excluded from three ranoid families (Brevicipidae, Hemisidae and Ptychanidae) as it lacks the osteological synapomorphies for all three families (Table 1). The other six ranoid families are currently lacking osteological synapomorphies (but not morphological, see Scott 2005; Frost et al. 2006), so we compared MA 11-3 to their South African members (Table 1). MA 11-3 can be excluded from the South African microhylids (*Phrynomantis*) and hyperoliids (*Phlyctimantis*) on cranial and postcranial osteological differences (Table 1). MA 11-3 is also excluded from three other families (Rhacophoridae, Arthroleptidae and Phrynobatrachidae) on the basis of cranial and postcranial differences (see Table 1). In general, the skeleton of MA 11-3 shares an overall resemblance with the South African *Amnirana* (Amniranidae) but can be excluded from this genus due to the shape and orientation of the transverse process of the third presacral vertebra (Table 1).

The tenth ranoid family present in South Africa is the Pyxicephalidae. We compared MA 11-3 to all known genera of this family. Our specimen can easily be excluded from the two genera *Microbatrachella* and *Arthrolepetella* due to the size differences (both genera are less than 25 mm long; Channing and Rödel 2019). Among the remaining genera, MA 11-3 is also excluded from *Cacosternum* Boulanger 1887, on the basis of both cranial and postcranial characteristics (Table 2). MA 11-3 differs from both *Natalobatrachus* and *Notophryne* on the shape of its scapula (Table 2) and from *Pyxicephalus* and *Aubria* by lacking any ornamentation on its dermal cranial bones and lacking an articulation between the squamosal and maxilla (Table 2; Clarke 1981). However, MA 11-3 does resemble the remaining pyxicephalid, and does not have any remarkable osteological differences with them (Table 2).

MA 11-3 shares numerous osteological characteristics with several pyxicephalid genera, mainly the presence of a median keel on the posterolateral expansions of the parasphenoid and a short sacral vertebra with cylindrical-like transverse processes that slightly widens distally. Pyxicephalids represent a very diverse family of sub-Saharan frogs spread across Africa (Clarke 1981; Channing and Rödel 2005). Unfortunately, the family currently lacks osteological synapomorphies (Frost et al. 2006; van der Meijden et al. 2011). A morphologically based phylogenetic analysis recovered several non-unique synapomorphies: (1) presence of an open groove for pathway of occipital artery on skull; (2) pars facialis of maxillae bearing slight ornamentation (absent in numerous pyxicephalids) and (3) digits II and III of forelimb of the same length (Lemierre et al. 2021). MA 11-3 status for all three characters is unknown. Hence, apart from overall similarities to pyxicephalids and osteological differences to all other South African families, there is currently no other arguments in favour of an assignment to pyxicephalids. Thus, we propose that MA 11-3 should be assigned to Ranoidea and ?Pyxicephalidae, to reflect this uncertainty.

Paleoecological implications

A preliminary study of the microfauna identified lagomorphs and rodents (*Dendromus* cf. *melanotis*, *Malacothrix makapani* and *Mystromys* cf. *hausleitneri*; F. Sénégas pers. com.) within Milo A. This seems to suggest, albeit with caution (the material is scarce), that the habitat was mainly composed of grassland. This hypothesis is also supported by the presence of two equids (*Eurygnathohuppus* and *Equus capensis*) and a suid (*Metridiochoerus andrewsi*) taxa (Pickford and Gommery 2020). In addition to this grassland environment, the presence of some bovid taxa, including a probable grazer (?Alcelaphinae) and *Tragelaphus*, likely suggests some patches of bush were present (Gommery et al. 2012). Furthermore, the presence of one element (a phalanx) of *Hippopotamus amphibius* indicates nearby sources of water (Gommery et al. 2012). Thus, the paleoenvironment of Milo A was likely a savannah. Most of the extant pyxicephalids are known to inhabit savannah and arid environments (Channing and Rodel 2019). Thus, the presence of a probable pyxicephalid in Milo A is coherent with the current paleoenvironmental interpretation.

In addition, anurans living in semi-arid environments (such as the one proposed here) are known to have developed various methods to survive the temperature variation, lack of freshwater or poorly oxygenated lakes (Aardt and Weber 2010). In pyxicephalid, the African bullfrog (*Pyxicephalus adspersus*) is known to build a cocoon made of shed skin to survive the dry season (Aardt and Weber 2010). For this dormancy period, anurans are known to seek subterranean burrows, with hypoxic conditions, to increase metabolic depression (Rossi et al. 2020). The position of the individual present in MA 11.3, with its forelimbs resting below the body and its hindlimbs folded, is similar to the one made by African bullfrog during dormancy (Loveridge and Crayé 1979). Thus, we suggest that the anuran preserved in MA 11-3 likely died during a period of subterranean dormancy, such as that undergone by *Pyxicephalus* during the dry season.

Conclusion

To conclude, the analysis of MA 11-3 allowed us to identify and describe the first articulated anuran skeleton from the Cradle of Humankind. The presence of a diplaceolous vertebral column allowed to assign MA 11-3 to the Ranoidea clade. Comparisons with members of all ranoid families from southern Africa revealed that MA 11-3 possess strong affinities with several pyxicephalid taxa, but until more information is made available, this attribution remains tentative. Interestingly, the position of the specimen suggests that the anuran may have died during a period of dormancy, as seen in *Pyxicephalus*.

Acknowledgements

The fieldwork at Bolt's Farm was funded by the Plio-Pleistocene Palaeontology section of the Ditsong: National Museum of Natural History, the IRL HOMEN (Hominids and Environments: Evolution of Plio-Pleistocene Biodiversity [Cradle of Humankind, South Africa]) of CNRS and NRF and the Pôle Sciences humaines et sociales, Archéologie et Patrimoine of the sous-direction de l'Enseignement supérieur et de la Recherche, French Ministry of Europe and Foreign Affairs via the Mission Paléoanthropologique Franco-Sud-Africaine (MPFSA). We also thank F. Sénégas (Sorbonne Université, CR2P, Paris) for the information concerning the microfauna of Milo A. We want to thank SAHRA (South African Heritage Resource Agency) for the permit, C. Klinkert (the landowner) for access to her property, S. Potze, former Ditsong National Museum of Natural History employee (now at La Brea, Los Angeles) for access to the specimen and J. Hoffman (NECSA, Johannesburg) for assistance with the tomography process of the specimen. Processing of tomographic data was undertaken at the 3D imaging facilities Lab of the UMR 7207 CR2P (MNHN CNRS UPMC, Paris). We thank Dr da Silva for his

editorial work and two anonymous reviewers for their comments that helped enhance this manuscript.

References

Boulanger GA. 1886. Quelques mots en réponse à la note de M. le Dr R. Blanchard sur la classification des batraciens. Bull. Soc. Zool. Fr. 11: 320–321.

Boulenger GA. 1917. Sur la conformation des phalangettes chez certaines Grenouilles d'Afrique. C R

Hebd Seances Acad Sci. 165: 987–990. https://doi.org/10.5962/bhl.part.1217.

Boulenger GA. 1887. Descriptions of new reptiles and batrachians in the British Museum (Natural History). Part III. Ann. Mag. Nat. Hist. 20(115): 50–53. https://doi.org/10.1080/00222938709460009.

Brain CK. 1958. The Transvaal ape-man bearing cave deposits. Pretoria: Transvaal Museum Memoir.

Brain CK. 1981. The hunters or the hunted? An introduction to African cave taphonomy. Chicago and London: The University of Chicago Press.

Broom R. 1936. New fossil anthropoid skull from South Africa. Nature. 138(3490): 486–488. https://doi.org/10.1038/138486a0.

Channing A, Boycott RC. 1989. A New Frog Genus and Species from the Mountains of the southwestern

Cape, South Africa (Anura: Ranidae). Copeia. 1989(2): 467–471.https://doi.org/10.2307/1445445.

Channing A, Rödel M-O. 2019. Field Guide to the Frogs & Other Amphibians of Africa. Penguin Random House South Africa.

Clarke BT. 1981. Comparative osteology and evolutionary relationships in the African Raninae (Anura Ranidae). Monit. Zool. Ital. Supplemento. 15: 285–331.

Cooke HBS. 1991. Dinofelis barlowi (mammalia, Carnivora, Felidae) cranial material from Bolt's Farm, collected by the University of California African expedition. Palaeont. afr. 28: 9–21.

Duellman WE, Trueb L. 1994. Biology of Amphibians. Baltimore: John Hopkins University Press.

Duméril C. 1805. Zoologie analytique, ou méthode naturelle de classification des animaux, rendue plus facile à l'aide de tableaux synoptiques. Paris: Allais.

Frost DR, Grant T, Faivovich J, Bain RH, Haas A, Haddad CFB, De Sá RO, Channing A, Wilkinson M,

Donnellan SC, et al. 2006. The Amphibian Tree of Life. Bull. Am. Mus. Nat. Hist. 297:1–291. https://doi.org/10.1206/0003-0090(2006)297[0001:TATOL]2.0.CO;2.

Gardner JD, Rage J-C. 2016. The fossil record of lissamphibians from Africa, Madagascar, and the Arabian Plate. Palaeobiodivers Palaeoenviron. Palaeoenvironments. 96(1): 169–220. https://doi.org/10.1007/s12549-015-0221-0.

Gómez RO. 2016. A new pipid frog from the Upper Cretaceous of Patagonia and early evolution of crown-group Pipidae. Cretac. Res. 62: 52–64. https://doi.org/10.1016/j.cretres.2016.02.006.

Gommery D, Badenhorst S, Sénégas F, Potze S, Kgasi L, Thackeray JF. 2012. Preliminary results converning the discovery of new fossiliferous sites at Bolt's Farm (Cradle of Humankind, South Africa). Ann. Ditsong Natl. Mus. Nat. Hist. 2: 33–45.

Haughton SH. 1931. On a Collection of Fossil Frogs from the Clays at Banke. Trans. R. Soc. S. Afr. 19 (3): 233–249. https://doi.org/10.1080/00359193109518836.

Hime PM, Lemmon AR, Lemmon ECM, Prendini E, Brown JM, Thomson RC, Kratovil JD, Noonan BP,

Pyron RA, Peloso PLV, et al. 2021. Phylogenomics Reveals Ancient Gene Tree Discordance in the Amphibian Tree of Life. Syst. Biol. 70(1): 49–66. https://doi.org/10.1093/sysbio/syaa034.
Lemierre A, Folie A, Bailon S, Robin N, Laurin M. 2021. From toad to frog, a CT-based reconsideration of Bufo servatus, an Eocene anuran mummy from Quercy (France). J. Vertebr. Paleontol. 41(3): e1989694. https://doi.org/10.1080/02724634.2021.1989694.
Loveridge JP, Crayé G. 1979. Cocoon formation in two species of Southern African frogs. S. Afr. J. Sci. 75: 18–20.
Lynch JD. 1971. Evolutionary Relationships, Osteology and Zoogeography of Leptodactyloid Frogs. Miscellaneous Publications, University of Kansas Publications, Museum of Natural History. pp 1–238.
Matthews T, Keeffe R, Blackburn DC. 2019. An identification guide to fossil frog assemblages of southern Africa based on ilia of extant taxa. Zool. Anz. 283: 46–57. https://doi.org/10.1016/j.jcz.2019.08.005.
Matthews T, Measey GJ, Roberts DL. 2016. Implications of summer breeding frogs from Langebaanweg, South Africa: Regional climate evolution at 5.1 mya. S. Afr. J. Sci. 112(9/10): 7. https://doi.org/10.17159/sajs.2016/20160070.
Matthews T, Steininger C. 2023. A new anuran genus from the fossil sites of Langebaanweg and Cooper's Cave, South Africa. Afr. J. Herpetol. 72(2): 163–189. https://doi.org/10.1080/21564574.2023.2251502.
Matthews T, van Dijk E, Roberts DL, Smith RMH. 2015. An early Pliocene (5.1 Ma) fossil frog community from Langebaanweg, south-western Cape, South Africa. Afr. J. Herpetol. 64(1): 39–53. https://doi.org/10.1080/21564574.2014.985261.
Pickford M, Gommery D. 2020. Suidos fósiles del Sistema paleokárstico de Bolt's Farm, Sudáfrica: implicaciones para la taxonomía y biocronología de Potamochoeroides y los Notochoerus. Estud Geol. (Madr). 76(1): 127. https://doi.org/10.3989/egeol.43542.536.
Rafinesque CS. 1814. Fine del prodromo d'erpetologia siciliana. Specchio delle Scienze, o, Giornale Enciclopedico di Sicilia. 2: 102–104.
Reig O. 1958. Proposiciones para una nueva macrosistemática de los anuros (nota preliminar). Physis. 21: 109–118.
Reynolds SC, Kibii JM. 2011. Sterkfontein at 75: review of palaeoenvironments, fauna and archaeology from the hominin site of Sterkfontein (Gauteng Province, South Africa). Palaeontol. afr. 46: 59–88.
Roček Z. 1980. Cranial anatomy of frogs of the family Pelobatidae Stanius, 1856, with outlines of their phylogeny and systematics. Acta. Univ. Carol Biol. 1980. 3: 1–164.
Rossi GS, Cramp RL, Wright PA, Franklin CE. 2019. Frogs seek hypoxic microhabitats that accentuate metabolic depression during dormancy. J. Exp. Biol. 223: 218743. https://doi.org/10.1242/jeb.218743.
Sanchíz B. 1998. Salientia. München: Pfeil.
Scott E. 2005. A phylogeny of ranid frogs (Anura: Ranoidea: Ranidae), based on a simultaneous analysis of morphological and molecular data. Cladistics. 21(6): 507–574. https://doi.org/10.1111/j.1096-0031.2005.00079.x.
Sénégas F, Thackeray JF, Gommery D, Braga J. 2002. Palaeontological sites on "Bolt's Farm", Sterkfontein Valley, South Africa. Ann. Transvaal Mus. 39: 65–67.
Smith A. 1849. Illustrations of the Zoology of South Africa; consisting breifly of figures and descriptions of the objects of Natural History collected during an expedition into the interior of South Africa, in the years 1834, 1835, and 1836; fitted out by "The Cape of Good Hope association for exploring Central Africa, Smith, Elder & Co. London: Smith, Elder & Co.

Thackeray JF, Gommery D, Sénégas F, Potze S, Kgasi L, McCrae C, Prat S. 2008. A survey of past and present work on Plio-Pleistocene deposits on Bolt's Farm, Cradle of Humankind, South Africa. Ann. Transvaal Mus. 45: 83–89.

Trueb L, Ross CF, Smith R. 2005. A new pipoid anuran from the Late Cretaceous of South Africa. J. Vertebr. Paleontol. 25(3): 533–547. https://doi.org/10.1671/0272-4634(2005)025[0533:ANPAFT]2.0.CO;2.

van Aardt WJ, Weber RE. 2010. Respiration and hemoglobin function in the giant African bullfrog Pyxicephalus adspersus Tschudi (Anura: Pyxicephalidae) during rest, exercise and dormancy. Afr. J. Herpetol. 59(2): 173–190. https://doi.org/10.1080/21564574.2010.521197.

van der Meijden A, Crottini A, Tarrant J, Turner A, Vences M. 2011. Multi-locus phylogeny and evolution of reproductive modes in the Pyxicephalidae, an African endemic clade of frogs. Afr. J. Herpetol. 2011;60(1):1–12. https://doi.org/10.1080/21564574.2010.523904.

van Dijk DE. 2003. Pliocene frogs from Langebaanweg, Western Cape Province, South Africa. S. Afr. J. Sci. 99: 123–124.

Vilakazi N, Gommery D, Kgasi L. 2020. First fossil Agama lizard discovered in the Cradle of Humankind (Bolt's Farm Cave System, South Africa). Ann. Ditsong Natl. Mus. Nat. Hist. 9: 6.

Wagler J. 1827. Untitled footnote. Isis von Oken. 20: 726.

Figure 1. Geographical maps of MA 11-3 location. **A**, Map of South Africa, with the Bolt's Farm palaeokarst system highlighted; **B**, picture of the Milo A site (IRL HOMEN/MPFSA-D. Gommery); **C**, 3D rendering of Milo A site (MPFSA-V. Pois).

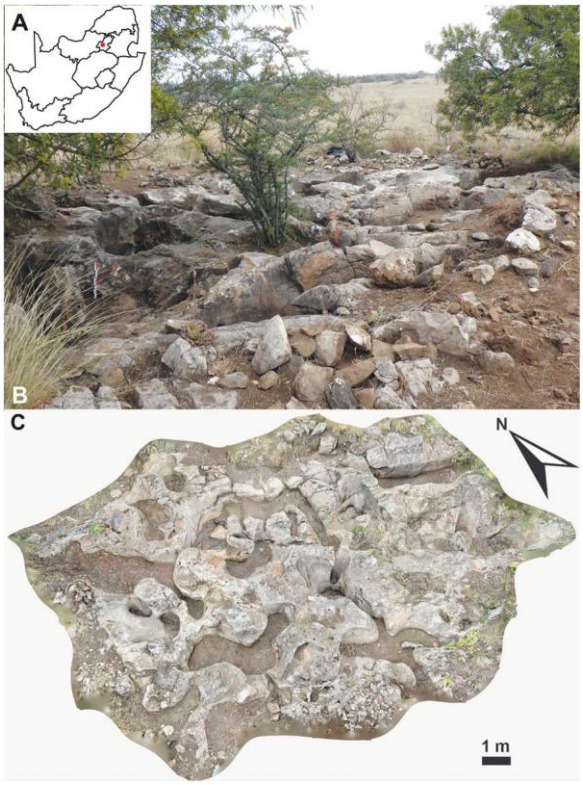

Figure 2. MA 11-3 and 3D model of the bloc. **A**, MA 11-3; and **B**, 3D-model of the cast of the cavity containing the skeleton, showing the body shape of MA 11-3, exposed in dorsal view. Outline represents the articulation between the atlas and the braincase (**A**), the sacro-urostylar articulation (**A**) and the orbital and nasal cavities (**B**). Scale bars represent 10 mm. **Abbreviations**: **ncp**, nasal capsule; **ob**, orbit.

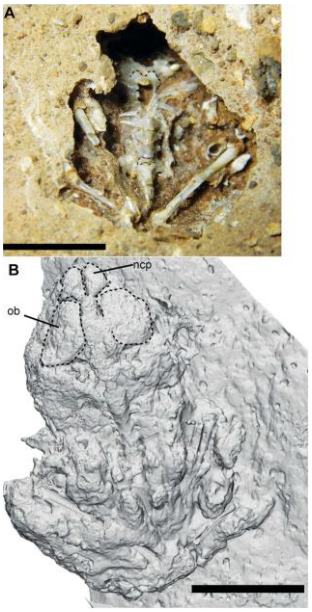

Figure 3. Articulated skeleton preserved in MA 11-3 exposed in ventral view. Scale bar represents 10 mm. **Abbreviations**: **asp**, angulosplenial; **dt**, dentary; **f**, femur; **fb**, fibulare; **hu**, humerus; **il**, ilium; **mtt**, metatarsal; **mx**, maxilla; **phx**, phalanx; **prs**, parasphenoid; **rdu**,radioulna; **sc**, scapula; **sph**, sphenethmoid; **sq**, squamosal; **tb**, tibiale; **tf**, tibiofibula.

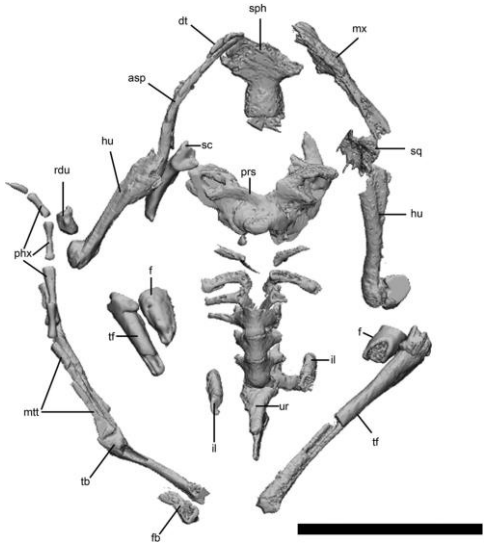

Figure 4. Cranial element of MA 11-3. **A**, Cranium of MA 11-3 in ventral view; **B-C**, left maxilla in **B**, labial and **C**, lingual views; **D**, incomplete left squamosal, showing its posterior region in labial view; **E**, right mandible in dorsal view; **F-G**, sphenethmoid in **F**, ventral and **G**, anterior views; and **H**, ventral region of the braincase, showing the parasphenoid and exoccipital. Scale bars represent 10 mm (**A**), and 1 mm (**B-H**). Outlines show the facet for articulation between pterygoid and parasphenoid (**A**) and palatine impression (**F**). **Abbreviations**: **asp**, angulosplenial; **at**, atlas; **cd**, crista dentalis; **cme**, crista mandibularis externae; **cpcrd**, crista paracoronoidea; **dt**, dentary; **exo**, exoccipital and prootic; **exs**, extremitas spatulate; **mx**, maxilla; **lh**, lamina horizontalis; **pab**, planum anteorbitale; **palimp**, palatin imprint; **pcrd**, processus coronoideus; **pf?**, processus frontalis?; **ppl**, processus posterolateralis; **psp**, parasphenoid posterolateral process; **qdjip**, quadratojugal imprint; **sam**; sella amplificans; **scm**, sulcus pro cartilagine Meckeli; **sn**, septum nasi; **sph**, sphenethmoid; **sq**, squamosal; **zr**, zygomatic ramus.

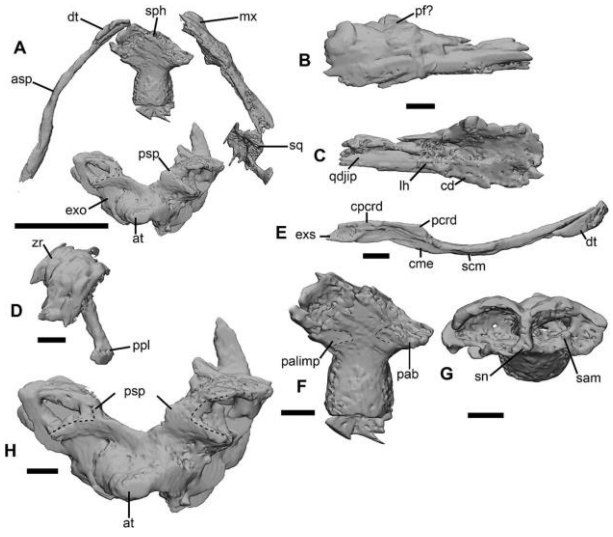

Figure 5. Postcranial elements of MA 11-3 (1). **A**, Partial articulated vertebral column in ventral view; **B**, posterior region of the column in lateral view; **C**, urostyle in lateral view; **D-E**, right scapula in **D**, lateral and **E**, medial views; **F-H**, left humerus in **F**, ventral, **G**, lateral and **H**, dorsal views. Scale bars represent 5 mm (**A**) and 1 mm (**B-H**). * highlights the glenoid fossa of the scapula. **Abbreviations**: **act**, anterior cotyle; **cpg**, crista pars glenoidalis; **cv**, crista ventralis; **dc**, dorsal crest; **dia**, diaphysis; **emc**, eminentia capitate; **er**, epicondylus raidale; **eu**, epicondylus unlare; **fc?**, fossa cubitalis; **ma**, anterior margin; **mp**, posterior margin; **mssp**, margin suprascapularis; **ols**, oleocranon scar; **pa**, processus acromialis; **pg**, processus glenoidalis; **stp**, sacral transverse process; **sv**, sacral vertebra; **tp**, transverse process; **II-VIII**, presacral vertebrae II to VIII.

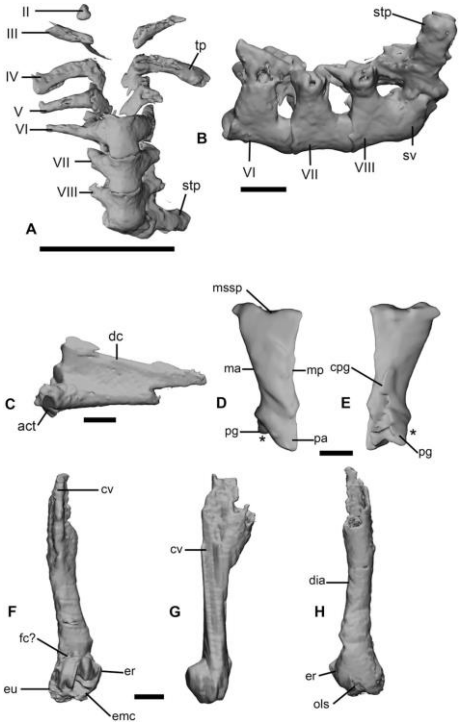

Figure 6. Postcranial elements of MA 11-3 (2). **A**, right hindlimb in lateral view and **B**, right foot in dorsal view, showing the different elements preserved. Scale bars represent 5 mm (**A**) and 2 mm (**B**). **Abbreviations**: **f**, femur; **fb**, fibulare; **mtt**, metatarsals; **mtt II-V**, metatarsals II to V; **phx t**, terminal phalanx; **phx I-III**, phalanx I to III; **tb**, tibiale; **tf**, tibiofibula.

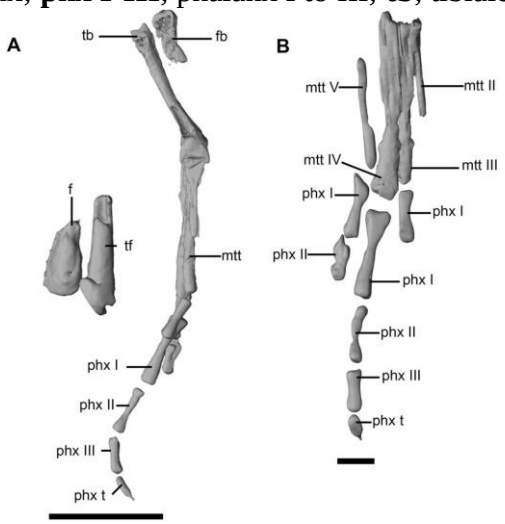

Table 1. Osteological comparison between MA 11-3 and nine ranoid families present in South Africa

Selected osteological characters	MA 11-3	Brevicipitidae / Hemisidae	Ptychadenidae	Microhylidae	Hyperoliidae	Rhacophoridae	Arthroleptidae	Phrynobatrachidae	Amniranidae
Cranium	Sphenethmoid united as a single element, floor of the nasal capsules ossified	-	-	sphenethmoid divided into two elements	sphenethmoid divided into two elements	-	floor of the nasal capsules poorly ossified	-	-
Vertebral column	Unfused V1 + V2; transverse process of V3 oriented posterolaterally to the vertebral axis unfused V8 and sacral vertebra; sacral transverse processes rod-like; well developed dorsal crest on the urostyle; anterior region of the urostyle wide	fused V1+V2; sacral transverse processes expanded distally; short dorsal crest on the urostyle	Fused V8 and sacral vertebra, with the transverse processes forming an X in dorsal view	short dorsal crest on the urostyle	-	anterior region of the urostyle narrow	anterior region of the urostyle narrow	Occipital cotyles widely separated	transverse processes of V3 oriented perpendicular to the vertebral axis
Forelimb	-	-	-	-	-	-	-	-	-
Hindlimb	elongated tibiofibula, tibiale and fibulare; cone-like terminal phalanges	-	-	forked terminal phalanges	-	-	-	-	-
Pectoral girdle	transversally elongated scapular shaft	-	-	transversally short scapular shaft	-	transversally short scapular shaft	-	[illegible] medial surface of the [illegible]	-

Table 2. Osteological comparison between MA 11-3 and all pyxicephalid genera.

Selected characters	MA 11-3	*Cacosternum*	*Natalobatrachus*	*Notophryne*	*Anhydrophryne*	*Tomopterna*	*Poyntonia*	*Pyxicephalus*	*Aubria*
Cranium	Ossified quadratojugal; no median keel on the posterolateral expansions of the parasphenoid; sphenethmoid ossified on at least half of its lenght; no ornamentation on its dermal bones; lamella alaris of the squamosal does not articulate with maxilla	Cartilaginous quadratojugal; median keel on the posterolateral expansion of the parasphenoid; sphenethmoid ossified on at least half of its lenght	Ossified quadratojugal; median keel on the posterolateral expansions of the parasphenoid; sphenethmoid ossified on at least half of its lenght; no ornamentation on its dermal bones; lamella alaris of the squamosal does not articulate with maxilla					Ossified quadratojugal; median keel on the posterolateral expansions of the parasphenoid; sphenethmoid ossified on at least half of its lenght; ornamentation on its dermal bones; lamella alaris of the squamosal articulates with maxilla	
Vertebral column	elongated transverse processes; centra protruding ventrally; rod-like sacral transverse processes; well-developed dorsal crest on the urostyle	short transverse processes; centra flattened ventrally; moderately expanded sacral transverse processes; short dorsal crest on the urostyle	elongated transverse processes; centra protruding ventrally; rod-like sacral transverse processes; well-developed dorsal crest on the urostyle						
Hindlimb	cone-like terminal phalanges	cone-like terminal phalanges	forked terminal phalanges	cone-like terminal phalanges					
Pectoral girdle	transversally elongated scapular shaft	transversally short scapular shaft	transversally elongated scapular shaft						